ELSEVIER

Journal of Alloys and Compounds 303–304 (2000) 454–464

Journal of ALLOYS AND COMPOUNDS

www.elsevier.com/locate/jallcom

A solid oxide fuel cell based on Sr- and Mg-doped $LaGaO_3$ electrolyte: the role of a rare-earth oxide buffer

Keqin Huang*, John B. Goodenough

Texas Materials Institute, The University of Texas at Austin, Austin, TX 78712, USA

Abstract

In this paper we review a systematic study on the properties of the superior oxide-ion conductor Sr- and Mg-doped $LaGaO_3$ (LSGM) and its performance in a single fuel cell. The conductivity of the oxygen-deficient perovskite phase was shown to be purely ionic over a wide range of oxygen partial pressures $10^{-22} \leq P_{O_2} \leq 1$ atm. The highest values of the oxide-ion conductivity, $\sigma_o = 0.17$, 0.08 and 0.03 S/cm, were found for $La_{0.8}Sr_{0.2}Ga_{0.83}Mg_{0.17}O_{2.815}$ at 800, 700 and 600°C, respectively; they remained stable over a weeklong test. The reactivity of Ni and LSGM suggested use of a thin interlayer at the anode–electrolyte interface to prevent formation of lanthanum nickelates; $Ce_{0.8}Sm_{0.2}O_{1.9}$ (SDC) was selected for the interlayer. The peak power density of the interlayered cell is 100 mW/cm^2 higher than that of the standard cell without the interlayer. This improvement is due to a significant reduction of the anode overpotential; the overpotential of the cathode $La_{0.6}Sr_{0.4}CoO_{3-\delta}$ (LSCo) remained unchanged. Comparison of the peak power density in this study and with that of a previous study, also with a 500-μm-thick electrolyte, indicates a factor of two improvement, i.e. from 270 mW/cm^2 to 550 mW/cm^2 at 800°C. The excellent cell performance showed that an LSGM-based SOFC operating at temperatures $T_{op} \leq 800$°C is a realistic goal.

Keywords: Solid electrolyte; Lanthanum gallate; Fuel cell; Solid oxide; Cathode; Anode; Buffer layer

1. Introduction

Realization of a commercially viable solid oxide fuel cell (SOFC) for use in a hybrid electric power plant depends on the identification of compatible materials for the electrolyte, electrode, and interconnect as well as on the fabrication techniques that optimize the kinetics of mass and electron transport through the bulk and across the several interfaces. Oxides with oxygen deficient fluorite and perovskite structures are key candidates since both structures allow oxide-ion conductivity at the desired operating temperatures ($600 < T_{op} < 800$°C) and can be either an electronic insulator or metallic. Moreover, rare-earth ions can be incorporated into each of these structures to modulate their physical properties.

Since Faraday's discovery of fast F^--ion conductivity in PbF_2, the search for anion conductors has concentrated on anion-deficient compounds with fluorite-related structures. As illustrated in Fig. 1, the fluorite structure consists of a face-centered-cubic cation array with anions in the tetrahedral sites. A small energy of excitation of the anion to a saddle-point position, located on the edge of an octahedron of cations between an occupied and an empty tetrahedral site, reduces the motional enthalpy ΔH_m for an oxide-ion jump within a (111) plane to a neighboring vacancy [1,2]. The oxide-ion conductivity increases with the concentration n_v of mobile oxygen vacancies as well as with the oxygen mobility $\mu \sim \mu_o \exp(-\Delta H_m/kT)$. The commercial oxide-ion electrolyte is yttria-stabilized zirconia, $Y_xZr_{1-x}O_{2-0.5x}$ (YSZ), and the government-sponsored SOFC projects have all taken YSZ as the starting point of a fuel-cell design. We have chosen to explore an alternative design based on a perovskite oxide-ion electrolyte, but we make use of the fluorite-related Sm_2O_3-doped ceria, $Sm_xCe_{1-x}O_{2-0.5x}$ (SDC), in our design.

The cubic ABO_3 perovskite structure is illustrated in Fig. 2. The smaller cation of the octahedral B sites may be a main-group or a transition-metal element; the larger A site may be occupied by a lanthanide, an alkaline earth, or an alkali atom. The tolerance factor $t \equiv (A–O)/\sqrt{2}(B–O)$ is a measure of the mismatch of the equilibrium A–O and B–O bond lengths. The structure adjusts to a $t < 1$ ($0.8 < t < 1$) by cooperative rotations of the $BO_{6/2}$ octahedra; the common rotations are about a cubic [111] or [110] axis,

*Corresponding author. Tel.: +1-512-471-4767; fax: +1-512-471-7681.

E-mail address: kqhuang@mail.utexas.edu (K. Huang)

0925-8388/00/$ – see front matter
PII: S0925-8388(00)00626-5

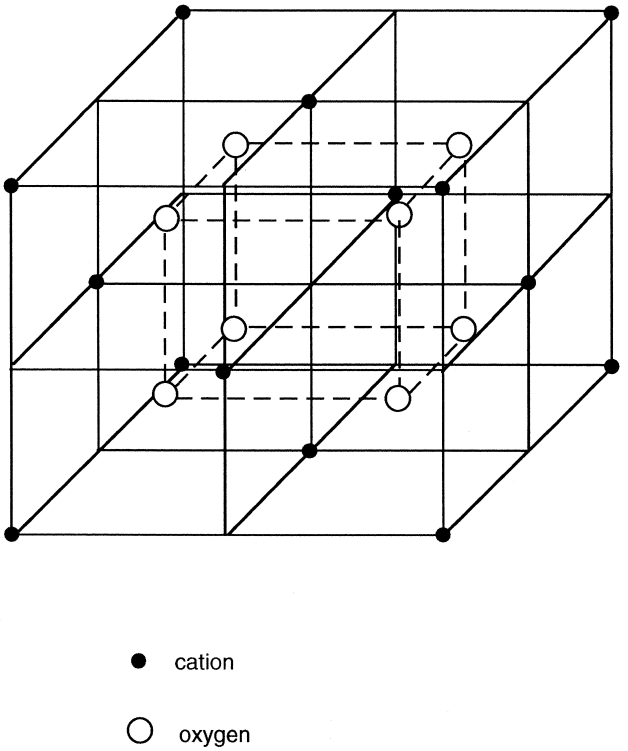

Fig. 1. The fluorite crystal structure.

which yield rhombohedral (R) and orthorhombic (O) symmetry, respectively. Buckling of the B–O–B bond angles to $(180^\circ - \phi)$ is greater for O than for R symmetry. The perovskite structure is extremely versatile. It not only tolerates a mismatch of the (A–O) and (B–O) equilibrium bond lengths, it also tolerates vacancies on any of the sub-lattices. Moreover, some transition-metal cations on the B sites support metallic conductivity of the BO_3 array, and the introduction of a mixed valency on the BO_3 array by aliovalent substitutions on the A sites introduces

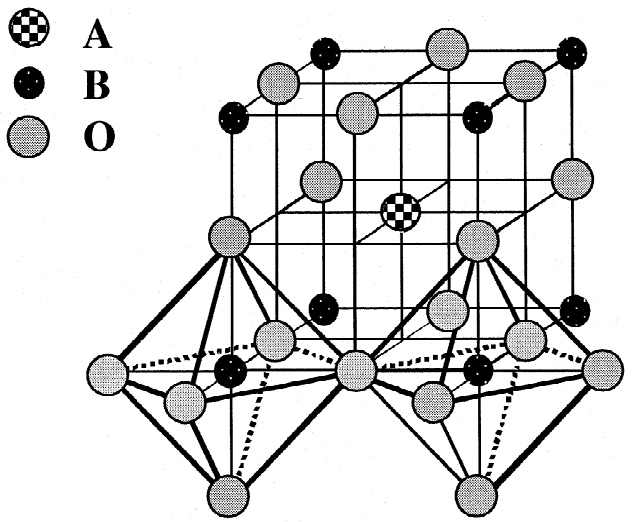

Fig. 2. The ideal perovskite primitive cubic crystal structure.

polaronic, if not metallic, electron transport even where the B-site cations carry a magnetic moment.

In order to demonstrate that the motional enthalpy of an oxide-ion in a perovskite can be as low as that in a fluorite, the oxide-ion conductivity $\sigma_o(T)$ was measured on heating $BaInO_{2.5}$ to above a first-order brownmillerite (ordered vacancies) to perovskite (disordered vacancies) transition at 930°C [3]. Subsequently, the perovskite Sr- and Mg-doped $LaGaO_3$ (LSGM) was shown to have an oxide-ion conductivity superior to that of YSZ with a transport number $t_o \equiv \sigma_o/\sigma \approx 1$ over the extended range of oxygen partial pressures encountered in a SOFC [4–6]. In this paper we report a systematic series of experiments aimed at optimizing the electrodes as well as the electrolyte for a SOFC that uses LSGM as the oxide-ion electrolyte.

2. Materials selection

2.1. The electrolyte

The solid oxide-ion electrolyte is the principal functional component of a SOFC. The chemical reaction driving a SOFC is split into anode and cathode reactions. For gaseous H_2 as the fuel, for example,

$$2\,H_2(g) + 2O^{2-} = 2\,H_2O + 4e^- \text{ (anode)}$$

$$O_2(g) + 4e^- = 2O^{2-} \text{ (cathode)}$$

The electrolyte transports the O^{2-} ions from the cathode to the anode, but it blocks electron transport, forcing the electrons of the reaction to traverse an external load. As a separator of the oxidant at the cathode and the fuel at the anode, it must be stable and transport only O^{2-} ions over oxygen partial pressures from 1 atm (oxidant) to 10^{-22} atm (fuel).

Minimization of the resistive losses of a SOFC requires a low electrolyte resistance $R = L/\sigma_O A$, where the oxide-ion conductivity is $\sigma_o \sim n_v \exp(-\Delta H_m/kT)$; L and A are the thickness and area of the electrolyte membrane. An operating temperature $T_{op} = 800$°C for a SOFC using YSZ as the electrolyte requires a thin ($L \sim 10$ μm) ceramic membrane. This constraint can be relieved considerably with LSGM as the electrolyte. Other resistive losses not considered in this estimate are the electrode/electrolyte interfacial resistances and the rates of the electrode reactions.

2.2. The anode

Nickel has been the anode of popular choice because of its high catalytic activity for the anode reaction and its relatively low cost. However, the anode reaction with nickel must take place at a three-phase nickel–fuel–electrolyte linear interface. Therefore, a composite NiO+

electrolyte anode is used with a YSZ electrolyte; the NiO is reduced to elemental nickel in the anode atmosphere, and the resulting porous structure not only provides the fuel access to a long three-phase interface, but also prevents coarsening of the metallic particles at the high T_{op}.

In our design with an LSGM electrolyte, we use a NiO+SDC composite so as to provide a mixed Ce^{4+}/Ce^{3+} valence for also catalyzing the anode reaction at the two-phase SDC–fuel interface [7].

2.3. The cathode

The cathode of a SOFC must perform three functions: (1) provide a mechanism for breaking the covalent bond of the O_2 oxidant molecule, (2) accept electrons from the external circuit and distribute them to the cathode reaction sites for the reduction of O to O^{2-}, and (3) transfer the O^{2-} ions to the electrolyte for transport to the anode where they oxidize the fuel in the anode reaction. These three functions can be realized in an oxide that conducts both electrons and oxide ions in the oxidizing atmosphere at the cathode.

Sr-doped $LaMnO_3$ (LSM) has been used extensively as the cathode material in a SOFC using a YSZ electrolyte. LSM has a close thermal expansion match to that of YSZ and a Mn^{4+}/Mn^{3+} mixed-valent MnO_3 array, which gives it a relatively high electronic conductivity in oxidizing atmospheres. However, LSM can only perform the first two functions of a cathode due to its lack of oxide-ion conductivity. Consequently, an LSM cathode must be fabricated with a fairly thick, porous microstructure containing percolation pathways for the oxidant as well as an extensive array of triple-phase linear interfaces where gas, electrolyte, and electrode meet. The performance of such a cathode depends sensitively on its microstructure, which may change under prolonged operating conditions. Depending on the microstructure, the cathode overpotentials have been reported to vary from a few tens to a few hundreds of millivolts. Clearly an alternate strategy based on a mixed ionic/electronic conductor (MIEC) is needed.

Sr-doped $LaCoO_3$, $La_{1-x}Sr_xCoO_3$ (LSCo), is a MIEC in an oxidizing atmosphere; it is difficult to oxidize Co(III) all the way to Co(IV). LSCo fulfills the three cathodic functions and has been demonstrated to give an excellent cathode performance with low overpotential even at high current density [7–9]. Unfortunately, the thermal expansion of the LSCo system is exceptionally high as a result of a change from low-spin Co(IV) to intermediate-spin Co(III) with the loss of oxygen on raising the temperature

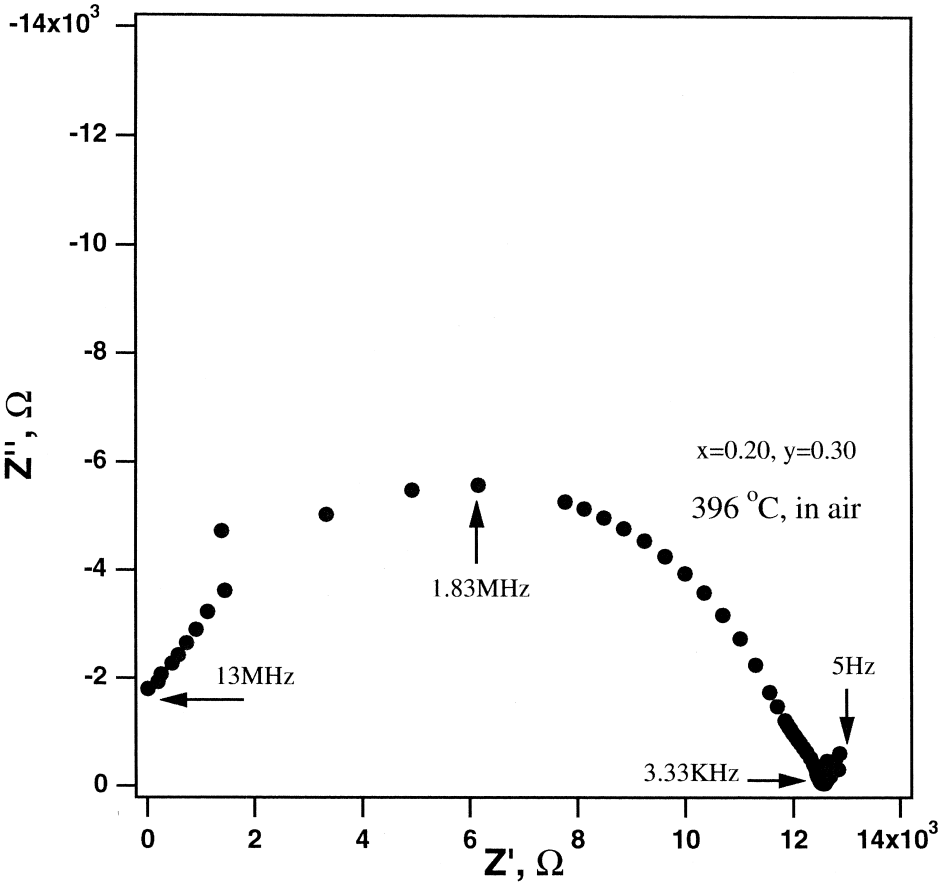

Fig. 3. Impedance spectrum of a $La_{1-x}Sr_xGa_{1-y}Mg_yO_{3-0.5(x+y)}$ sample with $x=0.2$, $y=0.30$ that contains $LaSrGaO_4$ as a second phase.

[10]. The thermal expansion mismatch between LSCo and the electrolyte, YSZ or LSGM, make this MIEC unsuitable as a cathode material for a SOFC subject to repeated thermal cycling. We have therefore identified recently two other perovskite systems that are MIECs with a closer thermal expansion coefficient (TEC), and we are testing these not only as possible cathodes, but also as membranes for gas separation [11].

2.4. The interconnect

In a SOFC stack, individual cells are connected in series; the interconnect is a conductor that contacts the cathode of one cell to the anode of an adjacent cell. Therefore, the interconnect material must be both chemically stable and electronically conductive at T_{op} in both the oxidizing and reducing atmospheres of the two electrodes. At the present $T_{op} \approx 1000$°C with a YSZ electrolyte, a ceramic interconnect, the Sr-doped $LaCrO_3$ perovskite, is used. However, with a $T_{op} = 800$°C, a stainless steel superalloy can be used provided the oxide scale that builds up at the cathode–interconnect interface remains conductive. Therefore, we have been investigating a superalloy that forms a conductive chromium-oxide scale in the cathode atmosphere [16].

3. Experimental procedures

3.1. Electrolyte preparation

Stoichiometric amounts of La_2O_3 (>99.99% purity), $SrCO_3$ (>99.9% purity), Ga_2O_3 (>99.99% purity) and MgO (>99.99 purity) were intimately mixed in an agate mortar with the aid of acetone. Before weighing, the La_2O_3 was fired at 1000°C for more than 3 h and MgO was obtained from the calcination of Mg carbonate (which appeared to be a mixture of carbonate and hydroxide) at 1000°C for more than 4 h. Pellets were made from the mixed powders under 200 MPa pressure and fired at 1250°C overnight. The partially sintered pellets were reground and ball-milled before a pellet 6 mm in diameter and 5–7 mm in length was made for measurement and

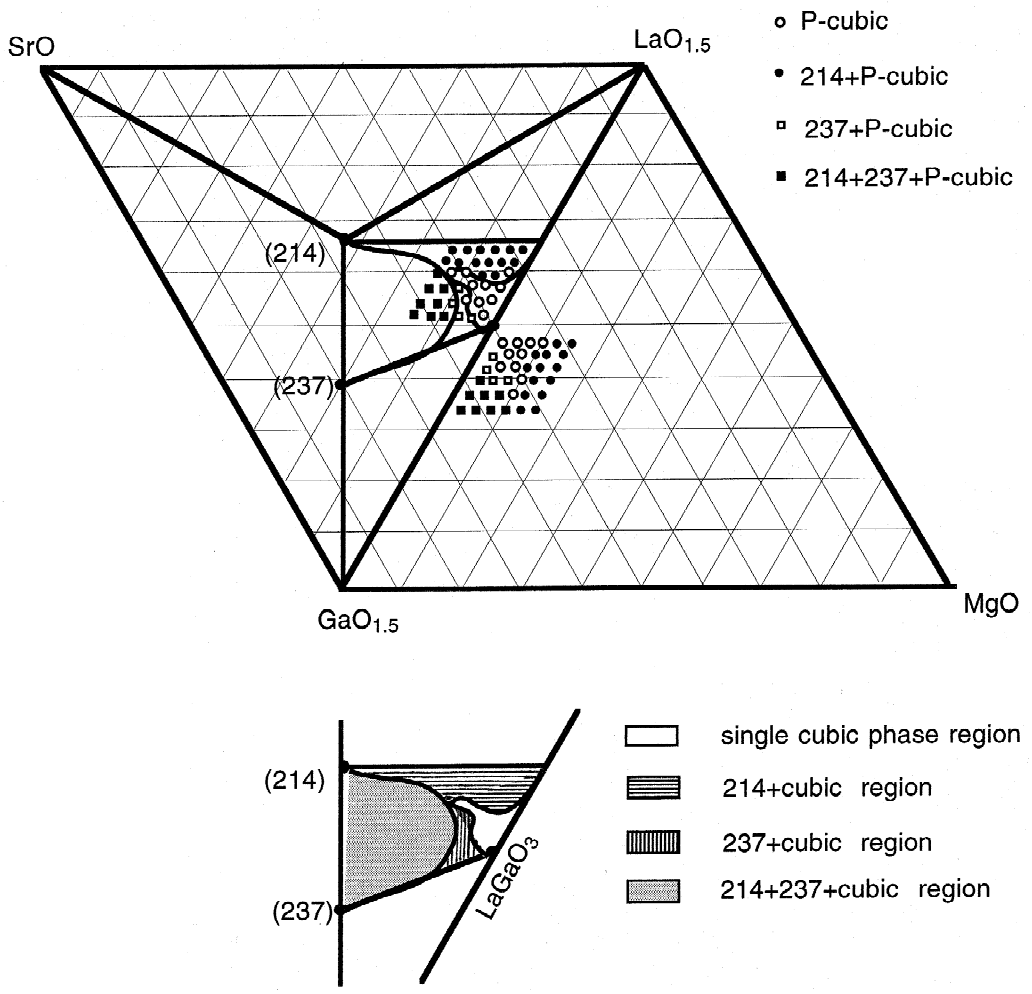

Fig. 4. Phase diagram of the $LaO_{1.5}$–SrO–$GaO_{1.5}$–MgO system.

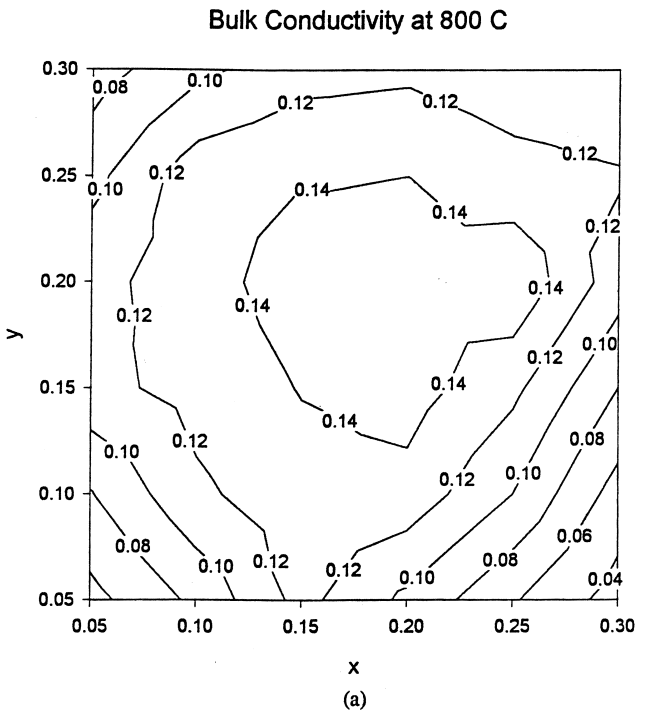

Fig. 5. Iso-conductivity plot of the LSGM compositions measured at 800°C in air.

sintered at 1470°C for 24 h. The final products were air-quenched from the furnace at 500°C.

3.2. Electrolyte characterization

The phases in the final products were determined by powder XRD with a Philips PW1729 diffractometer. Synthesized silicon powder was used as an internal standard for lattice-parameter determination. In order to monitor whether any existing impurities dissolved into the matrix at higher temperatures, high-temperature X-ray diffraction of single and multiphase samples was made with a Scintag model X1 high-temperature X-ray diffractometer. The high-temperature diffraction experiments were performed at 25, 600, 700 and 800°C with a scanning 2θ of 20–50°. In the Scintag X1 sample chamber, a platinum strip was used as both heater and supporter of the powder; X-ray lines from the platinum are present in the X-ray patterns because of the high X-ray penetration in this system. The raw diffraction data were refined by the Rietveld method.

The microstructures of well-polished pellets, sintered at 1470°C, were observed with a JSM-35C (JEOL, LTD) scanning electron microscope (SEM). The pellets were

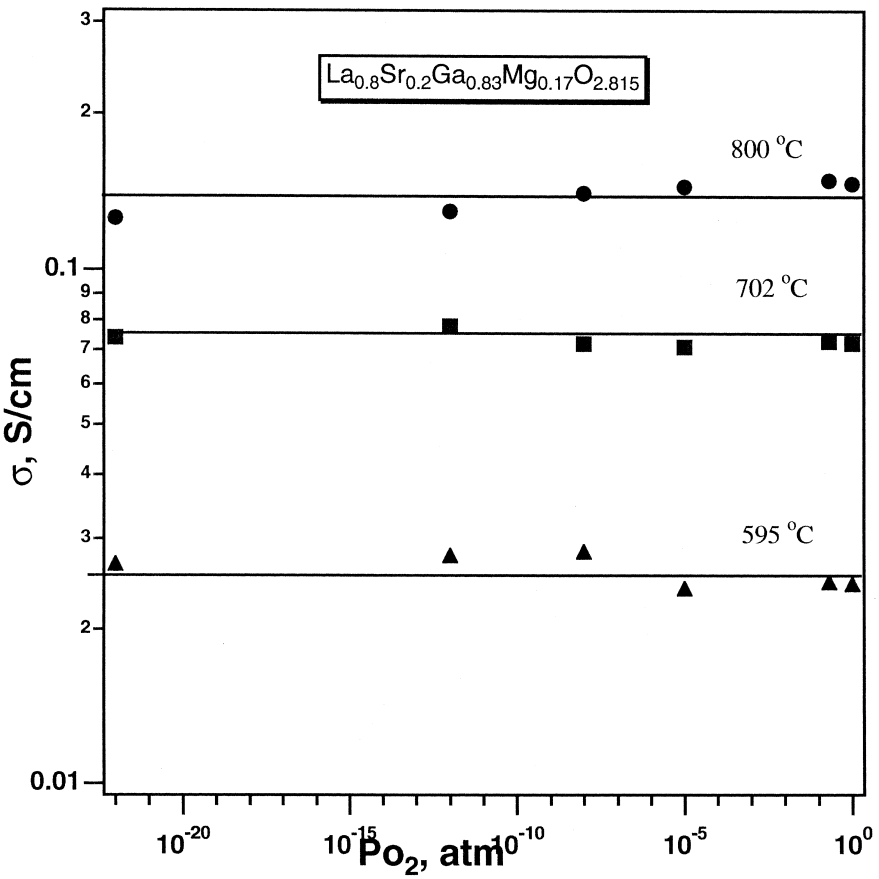

Fig. 6. Dependence on oxygen partial pressure of the conductivity of LSGM at several temperatures.

wet-sanded, polished, and then thermally etched for 1 h at 1350°C; a Pd–Au coating of the surface was used to prevent charging of the sample. In order to investigate grain-boundary effects, a transmission electron microscope (TEM) with a model JEM-200CX (JEOL, LTD) was used. The TEM samples were first ground to 100 μm thickness and were further thinned by ion milling. These membranes were sandwiched into two copper rings and fixed onto the TEM sample holder.

The ac conductivity of sintered pellets was obtained from two-probe impedance spectroscopy. The two electrodes were formed by applying platinum paste (Heraeus) to the two wet-sanded ends of the pellet and firing at 900°C for 30 min. Measurements were made with a Hewlett Packard 4192A LF Impedance Analyzer over a frequency range 5–13 MHz in the temperature range $320 \leq T \leq 800$°C (total of 25 experimental points) with an accuracy of ± 1.5°C at an ac voltage amplitude of 40 mV for all temperatures and all frequencies. The lead resistance, as obtained by measuring the impedance of a blank cell, was subtracted out from all the impedance measurements. Long-term conductivity stability was measured by impedance spectroscopy every 4 h at 700°C in air. Chemical stability was obtained by measuring the conductivity in different atmospheres ranging from pure oxygen to hydrogen saturated with water vapor.

3.3. Testing single fuel cells

In all of the single-fuel-cell tests, $La_{0.6}Sr_{0.4}CoO_{3-\delta}$ (LSCo) was used as the standard cathode material since it possesses both high oxide-ion and electronic conduction under cathodic conditions at lower temperatures. The anodes were formed by the reduction of 50:50 (volume percent) LSGM/NiO or SDC/NiO composites to give porous LSGM or SDC with metallic Ni particles on the walls of the porous channels. These composites represent standard anode materials for a SOFC, but with LSGM/Ni or SDC/Ni replacing YSZ/Ni. In order to avoid chemical interaction between the NiO of the anode and the LSGM electrolyte, an interlayer of SDC was applied between the LSGM electrolyte and the anode.

The overpotentials at both the cathode and the anode were monitored with reference electrodes constructed from the same materials and in the same way as the working electrodes. The electrodes and interlayer were fabricated on the top and bottom of a 500-μm-thick electrolyte membrane by screen-printing a slurry of an intimate

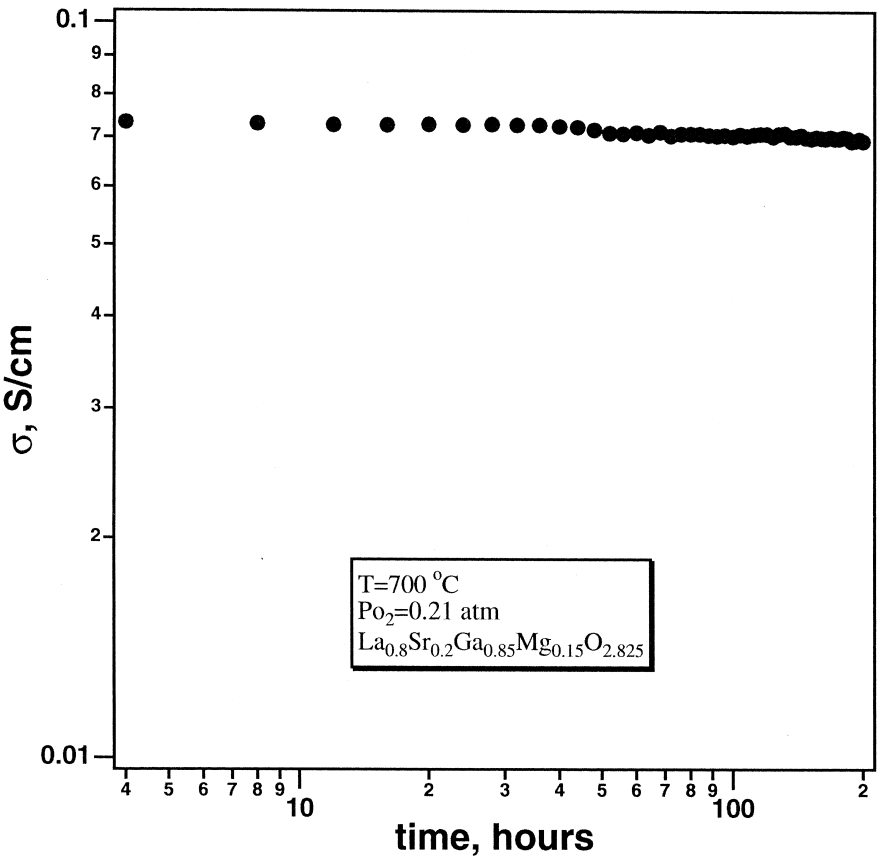

Fig. 7. Long-term stability of the conductivity of LSGM measured in ambient air at 700°C.

mixture of electrode powder and organic binder (from Heraeus). After baking at 1150°C for 2 h, Pt meshes with Pt leads were fixed, with an extra electrode paste to achieve good contact, on top of each electrode to act as current collectors. The effective electrode area was 2.5 cm^2. SEM observation gave a SDC interlayer thickness $\approx$10 μm. The cells were finally glass-sealed into zirconia tubes at 1100°C for 30 min since zirconia has a thermal expansion coefficient similar to that of LSGM. The glass sealant used for sealing the cells was developed by Ceramatec, Inc.

The test cells were placed in the hot zone of a vertical furnace. Air was supplied directly to the cathode surface; hydrogen (saturated with water vapor at ~25°C) was fed to the anode surface at a rate of 100 ml/min. All of the tests and the heating/cooling of the furnace were controlled by a computer; the tests were carried out in the temperature range $600 \leq T_{op} \leq 800$°C with an interval of 50°C. With a three-electrode configuration, typical *I–V* measurements were taken at a fixed temperature from open-circuit voltage (OCV) to 0.5 V and back to OCV in steps of 20 mV and holding 10 s at each point.

4. Results and discussion

4.1. The LSGM electrolyte

4.1.1. Impedance spectrum

Generally, the observation of impurities in a sample by X-ray diffraction signals the appearance of a grain-boundary contribution in the impedance spectrum. However, a typical sample, as shown in Fig. 3, revealed no grain-boundary semicircle even though a $LaSrGaO_4$ second

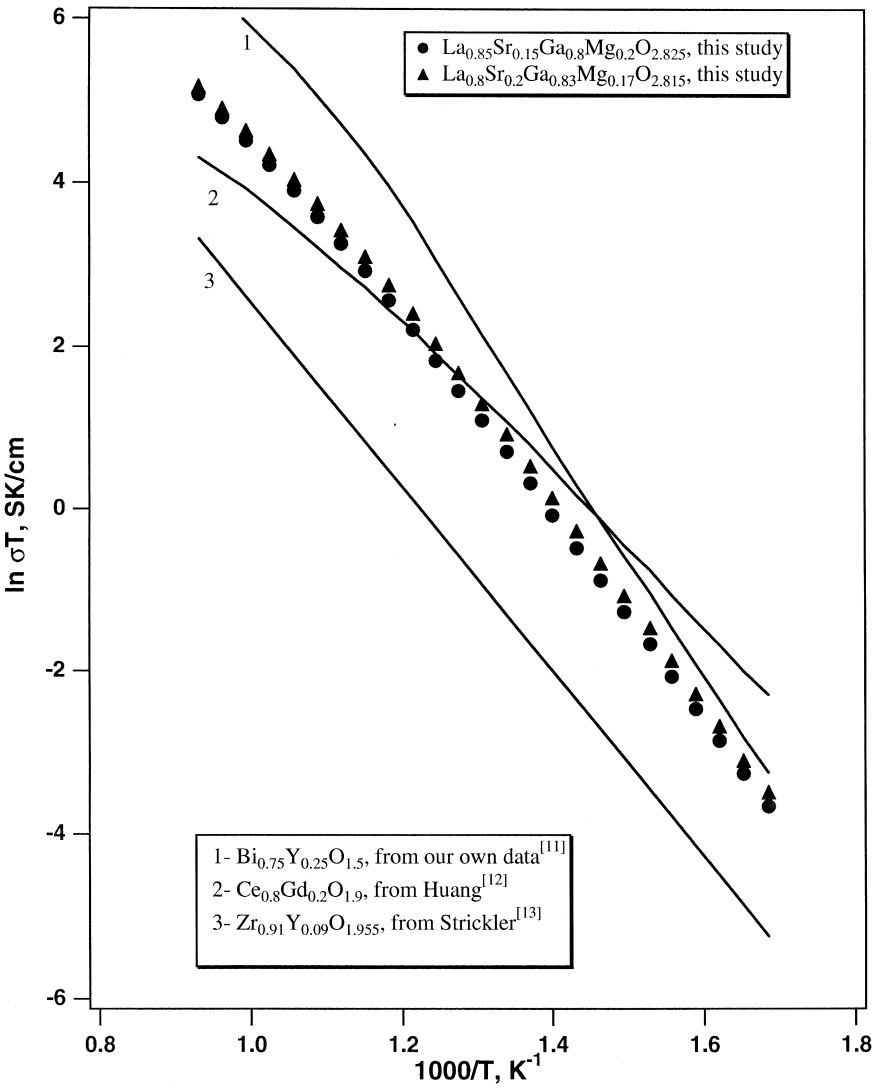

Fig. 8. Arrhenius plot of the conductivity of LSGM compared to some other well-known oxide-ion conductors.

phase was clearly detected by powder XRD. The related microstructures appear to indicate that a molten composition near $LaSrGaO_4$ that wets the grain boundaries can be attributed to the vanishing of the grain-boundary semicircle. This amorphous phase must be an oxide-ion conductor.

4.1.2. Phase relationships

Fig. 4 shows the quaternary $LaO_{1.5}$–SrO–$GaO_{1.5}$–MgO phase diagram constructed according to X-ray diffraction. High-temperature X-ray diffraction has also confirmed the validity of extending this diagram up to 800°C. Single-phase, two-phase, and three-phase regions were found, but no identified impurity containing Mg was found in the compositional range of Fig. 4, which implies a higher solubility of Mg in the perovskite phase. Preliminary studies show that the melting point of the doped $LaGaO_3$ perovskite is lowered as the Mg content increases until the MgO phase begins to segregate from the main phase. The amount of the low-melting-point compound $LaSrGaO_4$ increased with increasing Mg concentration.

4.1.3. Compositional dependence of σ_o

A typical contour plot of the conductivity at 800°C is shown in Fig. 5. The optimized composition in $La_{1-x}Sr_xGa_{1-y}Mg_yO_{3-0.5(x+y)}$ with the highest conductivity $\sigma_o = 0.17$ S/cm at 800°C is $x = 0.20$, $y = 0.17$. At this composition the sample remains a single phase without any grain-boundary contribution in the impedance spectrum.

4.1.4. P_{O_2} dependence and long-term stability of σ_o

In order to determine the transport number of the oxide-ion conduction, the conductivity in various oxygen partial pressures $1 \leq P_{O_2} \leq 10^{-22}$ atm was measured. Fig. 6 shows that the bulk conductivity of a typical composition $La_{0.80}Sr_{0.20}Ga_{0.85}Mg_{0.15}O_{2.825}$ is almost independent of oxygen partial pressure, which indicates pure oxide-ion conduction with negligible electronic conduction in this doped $LaGaO_3$ perovskite electrolyte. The long-term stability of the conductivity of the same composition was measured at 700°C in an atmosphere of air up to 1 week, as shown in Fig. 7. It is not surprising to see a stable conductivity since all the oxygen vacancies at 700°C are mobile; no ordering of oxygen vacancies contributes to the degradation of the conductivity as in the case of ZrO_2. Moreover, we did not find any carbonates or hydroxides in this perovskite electrolyte, probably because the constituent cations have stable coordination with the surrounding oxygen atoms, which minimizes any driving force to attract additional oxygen atoms into the lattice.

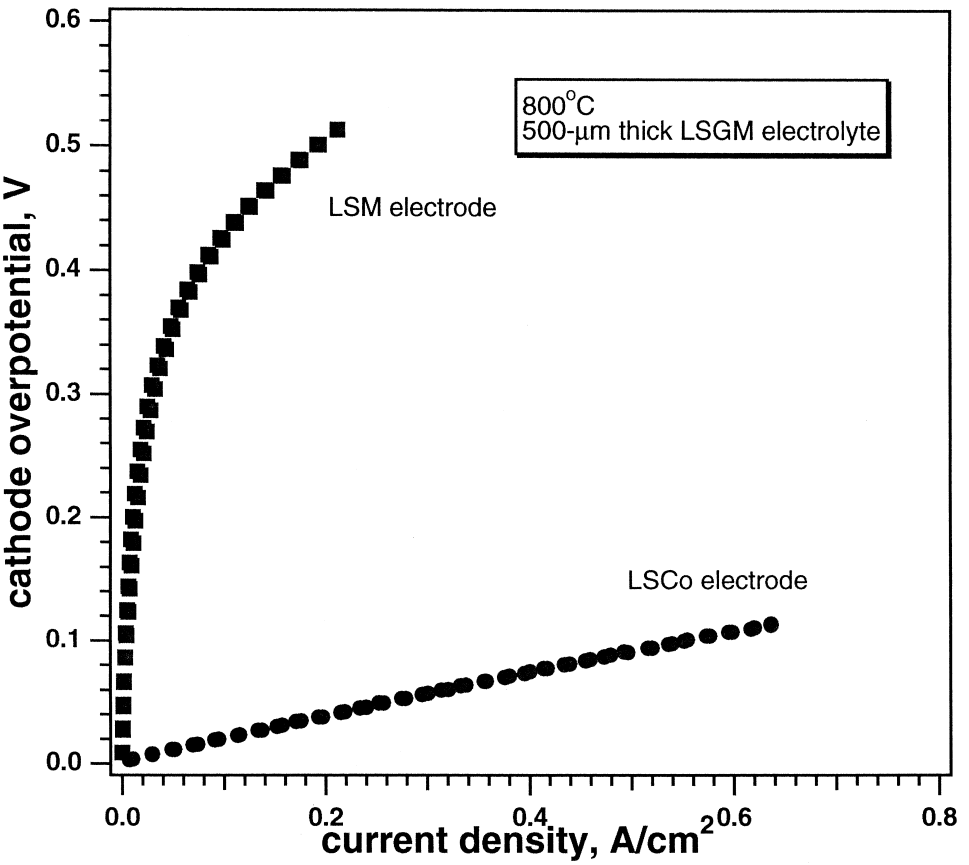

Fig. 9. Comparison of the LSCo and LSM cathode overpotentials at 800°C.

4.1.5. Temperature dependence of σ_o

The Arrhenius plots for two samples are compared in Fig. 8 with those for $Bi_{0.75}Y_{0.25}O_{1.5}$ [12], $Ce_{0.9}Gd_{0.1}O_{1.9}$ [13] and $Zr_{0.91}Y_{0.09}O_{1.955}$ [14]. The doped $LaGaO_3$ perovskites have a significantly higher σ_o at 800°C than do all other oxides except $Bi_{0.75}Y_{0.25}O_{1.5}$, which is unstable in the reducing atmosphere at the anode of a SOFC.

Fig. 8 also shows a curved Arrhenius plot; with increasing temperature the plot bends to a smaller activation energy $E_a = 0.82$ eV above 600°C from 1.08 eV below 600°C. We have interpreted this phenomenon as a condensation of oxygen vacancies into ordered clusters with decreasing temperature [6].

4.2. The cathodes

A significant interdiffusion between Ga and Co has been found across the LSCo/LSGM interface while almost negligible Ga–Mn interdiffusion occurs across an LSM/LSGM interface [17]. However, tests with a single fuel cell reveal a very low overpotential for the LSCo and a very high overpotential for LSM, see Fig. 9. It is evident that LSCo has a much higher exchange current i° than that of LSM whose I–η curve shows a significant electrode polarization. Obviously, mixed electronic and oxide-ion conductivity in LSCo plays a decisive role in lowering the electrode overpotential. Whether the observed interdiffusion between Ga and Co is beneficial to the decrease of the overpotential is under study. Unless specified otherwise, we use LSCo as a standard cathode in our fuel-cell tests. However, the large TEC of LSCo suggests that we investigate other MIECs with matching thermal expansion. Two such perovskites have been identified in our recent work [15].

4.3. The LSGM/anode buffer layer

We found a reaction occurs between Ni and LSGM at the fabrication temperatures T_f; an interfacial layer that is not an oxide-ion conductor blocks the fuel cell reaction [7]. In order to suppress this unwanted phase at the interface, we have chosen SDC as a buffer layer. Neither nickel nor the perovskite phase reacts with SDC at T_f or T_{op}, and the reducing atmosphere at the anode creates a mixed Ce^{4+}/Ce^{3+} valence in the SDC layer that helps to catalyze the dissociative chemisorption of the fuel. Reduction increases the oxygen-vacancy concentration of this fluorite phase, so

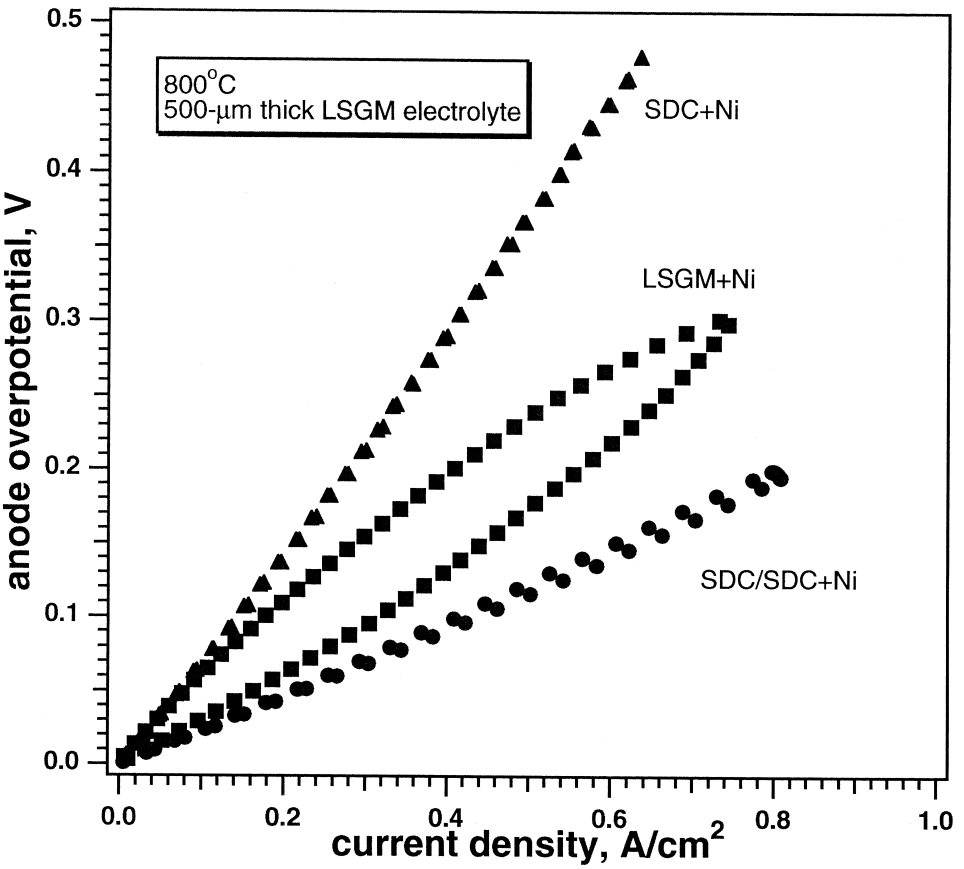

Fig. 10. Comparison of several anode overpotentials at 800°C with and without the SDC buffer layer. The LSGM+Ni overpotential is only shown for the initial cycle.

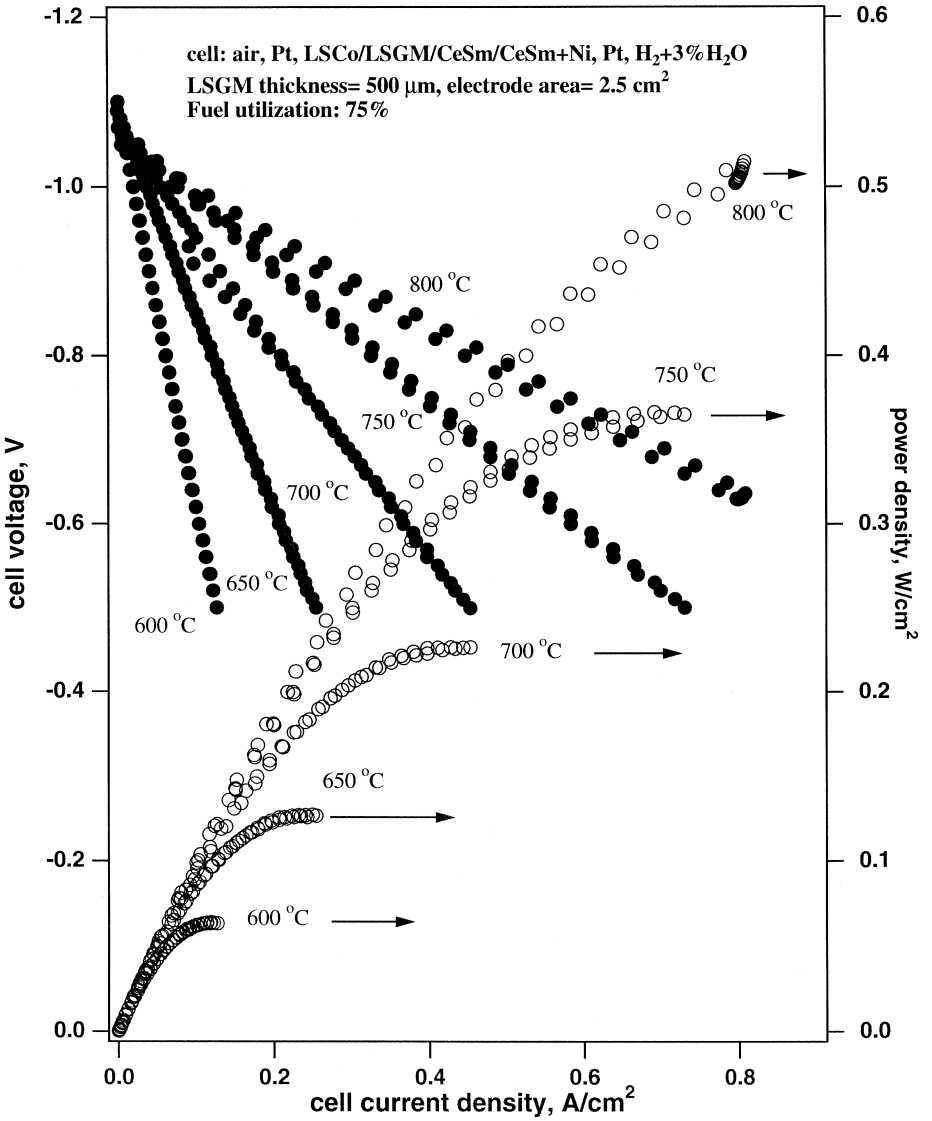

Fig. 11. Performance of a single fuel cell having a 500-μm thick LSGM electrolyte with a SDC buffer layer.

O^{2-}-ion transport occurs across the buffer layer to promote the fuel-cell reaction.

4.4. The anode

The need for a buffer layer indicates that the composite anode should be NiO+SDC rather than NiO+LSGM. The LSGM+Ni anodes proved to be unsuccessful; the electrode overpotential vs. current density of the first measurement is shown in Fig. 10. After several hours the overpotential of the LSGM+Ni anode surpassed that of the SDC+Ni anode and the power output was lowered to a minimum. In contrast, SDC+Ni anodes showed a stable value even though the overpotential remained relatively high compared to the initial value of LSGM+Ni anode.

With the addition of an SDC buffer layer, the overall anode overpotential is the lowest and stable, as shown in Fig. 10. As a consequence, the single cell with a 500-μm-thick LSGM gave a peak power density at 800°C of 550 mW/cm^2 with an SDC/SDC+Ni anode package, 440 mW/cm^2 with SDC+Ni and 270 mW/cm^2 with an LSGM+NiO anode, see Fig. 11.

5. Conclusions

Our experiments have shown that the single-phase composition $La_{0.8}Sr_{0.2}Ga_{0.83}Mg_{0.17}O_{2.815}$ is an oxide-ion solid electrolyte having a higher oxide-ion conductivity than YSZ and an electrolyte stability range covering the oxygen partial pressures encountered in a SOFC. It has a thermal expansion similar to that of YSZ, so electrodes

would appear to be interchangeable between the two electrolytes. However, LSGM reacts with Ni at the anode, so a thin buffer layer $Sm_xCe_{1-x}O_{2-0.5x}$ (SDC) is placed between the anode and the electrolyte and the anode composite becomes NiO + SDC rather than NiO + LSGM. Single-cell tests with a 500-μm-thick LSGM electrolyte show very promising performance compared to a YSZ electrolyte or a CeO_2 electrolyte at an operating temperature $T_{op} = 800$°C. A steady and high maximum power density 550 mW/cm^2 at 800°C was achieved with an LSCo cathode and a SDC + Ni anode having an electrolyte–anode interlayer of SDC. In the absence of an interlayer, an anode containing Ni obtained by reduction of NiO is prone to react with an LSGM electrolyte to form a lanthanum-nickel oxide; this surface reaction blocks the O^{2-}-ion transport needed for the fuel-cell reaction. The realization of a SOFC based on an LSGM electrolyte operating in the range $T_{op} \leq 800$°C appears to be a realistic goal. However, the evaluation of performance of alternate cathodes needs to be completed, the interconnect–electrode interfaces need to be studied in multicell tests, and improved fabrication techniques need to explored.

Acknowledgements

We thank EPRI (Electric Power Research Institute) and the Welch Foundation, Houston, Texas, for financial support.

References

[1] H.H. Mobius, Chemie 4 (1962) 100.
[2] J.B. Goodenough, Proc. Roy. Soc. (London) A393 (1989) 215.
[3] J.B. Goodenough, J.E. Ruiz-Diaz, Y.S. Zhen, Solid State Ionics 44 (1990) 21.
[4] T. Ishihara, H. Matsuda, Y. Takita, J. Am. Chem. Soc. 116 (1994) 3801.
[5] M. Feng, J.B. Goodenough, Eur. J. Solid State Inorg. Chem. T31 (1994) 663–672.
[6] K. Huang, R. Tichy, J.B. Goodenough, J. Am. Ceram. Soc. 81 (10) (1998) 2565–2575.
[7] K. Huang, R. Tichy, J.B. Goodenough, C. Milliken, J. Am. Ceram. Soc. 81 (10) (1998) 2581–2585.
[8] M. Feng, J.B. Goodenough, K. Huang, C. Milliken, J. Power Sources 63 (1996) 47–51.
[9] K. Huang, M. Feng, J.B. Goodenough, J. Electrochem. Soc. 144 (10) (1997) 3620–3624.
[10] M.A. Señarís-Rodrígues, J.B. Goodenough, J. Solid State Chem. 118 (1993) 223.
[11] K. Huang, M. Shroeder, J.B. Goodenough, Presented at 195th Electrochemical Society Meeting in Seattle, May of 1999. To be published in the Proceeding of Solid State Ionics and Devices.
[12] K. Huang, M. Feng, J.B. Goodenough, Solid State Ionics 89 (1996) 17–24.
[13] K. Huang, M. Feng, J.B. Goodenough, J. Am. Ceram. Soc. 81 (2) (1998) 357–362.
[14] D.W. Strickler, W.G. Carlson, J. Am. Ceram. Soc. 47 (1964) 122–127.
[15] K. Huang, H.Y. Lee, J.B. Goodenough, J. Electrochem. Soc. 145 (9) (1998) 3220–3227.
[16] K. Huang, P. Hou, J.B. Goodenough, accepted to be published in the memorial issue for Professor P. Kofstad of Solid State Ionics.
[17] K. Huang, M. Feng, J.B. Goodenough, M. Schmerling, J. Electrochem. Soc. 143 (10) (1996) 3630–3636.